

FORMATION CONTROL OF A ROTORCRAFT MULTI-LIFT SYSTEM

Jacob Enciu, Joseph F. Horn, Jack W. Langelaan
 Department of Aerospace Engineering, The Pennsylvania State University,
 University Park, PA 16802

Abstract

The formation dynamics and control of a four rotorcraft multi-lift system is presented. The uncontrolled system is shown to be inherently unstable and dynamically complex. A dynamic inversion controller is developed, and modified from a controller developed in previous work. The modified controller eliminates the need for sling cable forces feedback, enforces safe separation in the formation, and includes rotorcraft/load heading coordination functions. Simulations of the controlled system show that the multi-lift system can be successfully controlled by a single pilot. Simulation results suggest that optimization of formation geometry can provide improved system efficiency and handling qualities.

NOTATION

A, B, C	= system linear model matrices	$\theta_{1C}, \theta_{1S}, \theta_0, \theta_{TR}$	= lateral, longitudinal, collective and tail pitch angles
C_S	= cable damping coefficient	χ	= trajectory heading angle
e	= tracking error dynamics	ψ, θ, ϕ	= yaw, pitch and roll angles
\vec{F}_S	= cable tension force	ω	= frequency
\vec{f}	= function vector	$()_F$	= fuselage
h	= attitude	$()_H$	= helicopter
K_P, K_I, K_D	= proportional integral and differential gain matrices	$()_L$	= load
K_S	= cable stiffness	$()_{N,E,D}$	= north, east, down
l	= cable length	$()_R$	= main rotor
m_L	= load mass	$()_S$	= system
m_{REF}	= mass of reference load	$\dot{\square}$	= time derivative in an inertial coordinate system
n	= scale factor	$\hat{\square}$	= unit vector
p, q, r	= roll, pitch and yaw rates		
r	= reference signal		
t	= time		
u	= control commands vector		
u, v, w	= inertial velocity components		
V	= formation velocity		
X_A, X_B, X_C, X_P	= lateral and longitudinal stick, collective, pedals		
x, y, z	= longitudinal, lateral and vertical position		
\vec{x}	= state vector		
x	= linear model state vector		
$\beta_0, \beta_{1S}, \beta_{1C}$	= main rotor flapping angles		
$\Delta, \Delta x, \Delta y$	= absolute, longitudinal and lateral separation distances		
Δl	= cable stretch		
ζ	= damping ratio		
$\lambda_0, \lambda_{1S}, \lambda_{1C}$	= dynamic inflow components		
v	= pseudo control vector		

1. INTRODUCTION

External carriage of underslung loads by rotorcraft permits efficient aerial transportation of large and heavy loads, and their quick loading and unloading. This allows the resupply of needed equipment to places for which transport by land is impossible or limited due to topographical, meteorological or other conditions. The maximal external load that can be carried by a single rotorcraft is usually limited by either aerodynamic performance or structural strength limitations. As a result, the carriage of large loads requires utilization of heavy-lift military helicopters (that are not always available). When carriage of even larger loads is required, the only alternative that currently exists is the partition of this load into lighter separate sections that are each within the rotorcraft slung load carriage envelope.

Common carriage of a single load by multiple rotorcraft can enable carriage of much larger and heavier loads, than is currently possible using a single rotorcraft. However, despite the clear advantages of multi-lift carriage, the system's complexity and the high degree of coupling between the helicopters and

the load create significant engineering challenges. These are required to be overcome before such a system can be realized. The main difficulties in multi-lift carriage of loads lie in the need to determine the fundamental stability characteristics of such a system, and to provide means for its safe control. A safe and efficient control strategy is required to either enable the design of an efficient controller which will fly the system (in case of an autonomous system), or provide acceptable workload for the pilots operating the rotorcraft comprising the formation (when the system is manned).

Due to the described potential of the multi-lift concept, studies have been conducted in the past regarding multi-lift carriage. However, the concept has not materialized into a widely used operational system (an exception being the ad-hoc use of dual lift by various operators such as those in the lumber industry – Fig. 1 [1]). The renewed interest in the multi-lift concept in recent years is a direct result of the maturity of controls and automation technology using advanced sensors and sophisticated control algorithms. Such technology is currently being fielded to minimize pilot workload on manned rotorcraft and to achieve fully autonomous operation of unmanned rotorcraft.

The two basic configurations for multi-lift carriage are demonstrated in Fig. 2 [2]. In the pendant configuration (Fig. 2a) the sling cables are directly connected to the helicopters. This type of arrangement simplifies the required equipment for underslung load carriage, but creates significant workload to the pilots due to the need to keep the

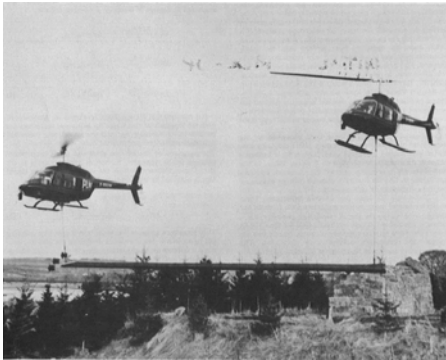
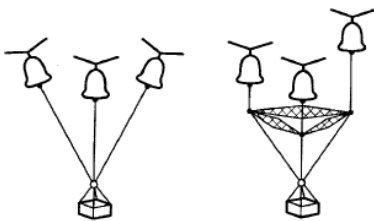


Fig. 1. Two Bell 206 JetRangers twin-lifting a log [1]



a) pendant b) spreader bar

Fig. 2. basic configurations for multi-lift carriage [2]

rotorcraft safely separated. In addition, the cables must be angled to maintain safe separation, resulting in some loss of lift capability. The spreader bar configuration (Fig. 2b) reduces the pilot workload by using a stiff structure that keeps the helicopters apart. However, this comes with the added weight and drag of the spreader bar structure that reduces the system's efficiency, and operational flexibility.

Multi-lift carriage has been studied in the helicopter industry and in academia since 1957 [3]. In 1970, a report describing a flight demonstration of two CH-54B helicopters lifting a load of 35,000 lb was published by Sikorsky Aircraft Co. [4]. This demonstration utilized a spreader bar configuration, and was limited to very slow forward flight speeds. The twin lift concept was also demonstrated by the USSR using MIL-26 helicopters, and a few others. However, high pilot workload issues and flight safety concerns prevented the further development of such systems.

Multi-lift systems of various arrangements have been studied by several researchers. Most of the work concentrated on dynamic analysis of the coupled rotorcraft/slung load dynamics [2], and investigations of the basic system's stability and control characteristics [1,5-7]. These have shown that the manual control of a multi-lift formation will involve high pilot workload and will adversely affect the system's flying qualities. The increased workload was attributed to the high bandwidth required for stabilizing the system, as well as the need to sense and utilize helicopter separation throughout the maneuver [6]. As a result, it was concluded that stability and command augmentation systems would be required for operation with tolerable workload. It should be mentioned that the majority of these efforts examined a twin lift configuration utilizing a spreader bar for the carriage of a single external load. Controllers aimed at augmenting system stability and reducing pilot workload have been proposed and analysed using linear and nonlinear simulations [8, 9]. The challenges of developing a flight formation of multiple unmanned rotorcraft was introduced in [10], and preliminary results of the formation control of multiple unmanned rotorcraft were presented.

Recently, a simulation model of a multi-lift rotorcraft system was developed and demonstrated for a formation of four utility helicopters (similar to a UH-60 Black Hawk) carrying a single load [11]. The sling cables were attached to the load at four different locations, such that the formation could control the attitude and position of the load. A nonlinear controller was designed using the method of dynamic inversion demonstrated in previous work [12-14]. The controller was shown to have the capability to track a required trajectory representing a complex maneuver of the system. More recently, a linear state feedback

controller was developed that achieved coordinated control of four unmanned rotorcraft using object based control methods developed in the robotics community [15]. Both of these design efforts demonstrated the capability of performing detailed maneuvers in 3D space. However, both designs require the capability of real time measurement of the sling cables tensions for use as feedback signals. In addition, no dedicated logic aimed at maintaining safe separation distances between the formation helicopters had been included in the designs.

The simulation model described in Ref. [11] was recently further enhanced to include more realistic load and sling cables properties. The dynamic inversion (DI) controller was redesigned so that cable tension measurements are no longer needed as inputs to the control system. In addition, safe separation and payload/formation relative heading keeping control laws have been added to the controller design. The current paper presents the development of this enhanced simulation model and presents the results obtained using it. At first, the uncontrolled system's dynamic model is presented, and its dynamics analysed. Then, the modified DI controller is described. The need for the implementation of the added control laws is explained, and the improvements resulting by their addition are presented. The controlled system's capability of following a complex maneuver is then demonstrated, by the addition of a trajectory control command generator. Finally, the conclusions of this work are presented, with recommendations for further research proposed.

2. SYSTEM MODELING

The system is comprised of four identical utility helicopters (similar to a UH-60 Black Hawk) carrying a single large slung load. The load's weight and size exceed the limits for single helicopter carriage. The helicopters are positioned at the corners of a 100x100 ft square. Each corner on the load's upper face is connected to one of the carrying helicopters cargo hook using a 200 ft sling cable. Figure 3 shows the general layout of the system's geometry.

2.1. Load Model

For the current research, it was assumed that the carried slung load is a 20,000 lb cargo container, similar in shape to a standard CONEX cargo container. This 8x6x6 ft boxlike military load is currently limited to 60 Knots during single carriage flight due to load instability problems. Therefore it was extensively studied through computational fluid dynamics (CFD) analyses, static and dynamic wind tunnel tests and flight tests [16-23] that provided comprehensive data that can be utilized in the current research. Figure 4 shows the carriage of this load by

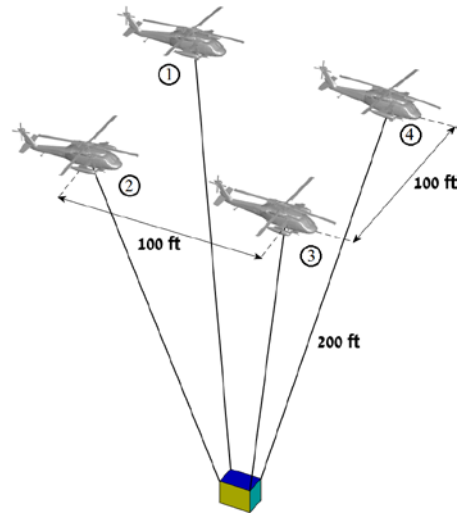


Fig. 3. Multi-lift system layout



Fig 4. Single carriage of the CONEX cargo container by a UH-60L Black Hawk [21]

a UH-60L Black Hawk helicopter during flight tests conducted by the US Army AeroFlightDynamics Directorate (AFDD) [21].

The current load's geometric and inertial properties were scaled up using Froude scaling rules [19]. A scale factor n of 1.64 was calculated from the mass ratio of the current load to that of the reference CONEX container (4532 lb):

$$n = \sqrt[3]{\frac{m_L}{m_{REF}}} \quad (1)$$

The load's aerodynamic model is based on the CONEX static aerodynamic coefficients obtained through wind tunnel tests [16]. The load's geometric center is used as a reference point for determination of the inertial velocity components (which determine the angle of attack, sideslip angle and dynamic pressure). The model is quasi-steady and does not account for any unsteady aerodynamics effects. This assumption is justified by the very low angular rates that are developed by the load during slung carriage due to the inherent stiffness of the particular studied

configuration. Specifically, the attachment of the four sling cables to four separate “corners” of the rotorcraft formation results in significantly higher yaw stiffness as compared to that during single helicopter carriage. This precludes the development of significant load yawing motions that are the main driver of the unsteady aerodynamic effects of bluff bodies. The equations of motion are implemented as a state space model with the state vector being comprised of the load’s angular rates, Euler angles, inertial velocities and center of gravity position:

$$\vec{x}_L = \left\{ p_L, q_L, r_L, \psi_L, \theta_L, \phi_L, u_L, v_L, w_L, x_N, y_E, z_D \right\} \quad (2)$$

The angular rates and inertial velocities are given in a load fixed coordinate system (L) located at the center of gravity, with the x axis pointing forward, y axis pointing right and z axis pointing down. The position vector is given in an earth fixed NED inertial system (E), with the x axis pointing to the north, y axis pointing to the south, and z axis pointing down. The transformation from this earth fixed coordinate system to the load fixed coordinate system follows the conventional “321” order of Euler angles rotation:

yaw (ψ_L) → pitch (θ_L) → roll (ϕ_L).

2.2. Sling Cables Model

Four identical sling cables of 200 ft length are connecting the load to the helicopters cargo hooks. Each cable is modeled as a linear spring and damper combination, assumed to hold only a tension force. The tension force in i^{th} cable is calculated from the cable’s stretch, Δl_i , and its rate of change, and is directed along the cable’s unit length vector:

$$\vec{F}_{S,i} = \max(K_{S,i} \cdot \Delta l_i + C_{S,i}(\dot{\Delta l}_i), 0) \cdot \hat{l}_i \quad (3a)$$

Where:

$$\hat{l}_i = \frac{\vec{l}_i}{|\vec{l}_i|} \quad (3b)$$

For the case when the cable suspension points are fixed, the cable vectors can easily be expressed as a function of the load’s position, attitude and geometric properties. These vectors directions are defined positive for vectors originating from the fixed suspension points and pointing into the load’s corners. Stiffness and damping values of 21,788 lb/ft and 99.4 lb-sec/ft were used for $K_{S,i}$ and $C_{S,i}$, respectively. In addition to the assumption that no compression forces are carried by the cables, it is also assumed that no bending and torsion moments are transmitted through them. Therefore cargo hook and load to cables attachment points are considered as spherical frictionless joints. As will be shown later, this conservative assumption leads to some

difficulties in modelling the slung load’s trajectory. When the load is carried by the rotorcraft, the cargo hook positions change with time, and can be calculated using the rotorcraft position, attitude and geometric properties.

2.3. Helicopter Model

The current research utilized the utility helicopter model of a UH-60 Black Hawk described in Ref. 11. Although the simulation model was modified in order to allow future investigations with mixed helicopter formations, four identical helicopter models are currently used. The helicopter nonlinear model is largely based on the GENHEL engineering simulation of the UH-60 helicopter [24]. The main rotor model employed is more simplified as compared to the original simulation as it neglects the blade lag dynamics, uses a linear lift aerodynamic model for the blade sections, and utilizes approximate closed form expressions for the main rotor total hub aerodynamic loads. The model follows Ref. 25, but uses a hinge offset representation rather than a center spring model. The dynamic inflow model used is that of Pitt-Peters [26]. The helicopter’s automatic flight control system was not included in the model, because a dedicated controller will be later added to the system in order to provide the desired stability and control characteristics.

As for the load, the helicopter model is implemented as a state variable model. The 21 element state vector of the i^{th} helicopter, $\vec{x}_{H,i}$, is comprised of a 12 element rigid body state vector, $\vec{x}_{F,i}$, and a 9 element main rotor state vector, $\vec{x}_{R,i}$, as follows:

$$\vec{x}_{F,i} = \left\{ u_H, v_H, w_H, p_H, q_H, r_H, \psi_H, \theta_H, \phi_H, x_H, y_H, z_H \right\}_i \quad (4a)$$

$$\vec{x}_{R,i} = \left\{ \beta_0, \beta_{1S}, \beta_{1C}, \dot{\beta}_0, \dot{\beta}_{1S}, \dot{\beta}_{1C}, \lambda_0, \lambda_{1S}, \lambda_{1C} \right\} \quad (4b)$$

$$\vec{x}_{H,i} = \left\{ \vec{x}_{F,i}, \vec{x}_{R,i} \right\} \quad (4c)$$

Similar to the load, the angular rates and inertial velocities for the i^{th} helicopter are given in a fuselage fixed coordinate system (Hi) located at the helicopter’s center of gravity. The helicopter’s position vector is given in the earth fixed coordinate system (E). The transformation from (E) to (Hi) follows the conventional order of yaw, pitch and roll Euler angles, $\psi_{H,i}, \theta_{H,i}, \phi_{H,i}$. The main rotor’s state vector is composed by the tip path plane’s first harmonic flapping angles and their rates of change, and by the main rotor’s dynamic inflow components.

2.4. Complete System

The equations of motion (EOM) for the complete

system are received by combining the load's EOM with four sets of helicopter EOM, one set per helicopter. The resulting set of state equations has the following form:

$$\begin{bmatrix} \dot{\vec{x}}_L \\ \dot{\vec{x}}_{H,1} \\ \dot{\vec{x}}_{H,2} \\ \dot{\vec{x}}_{H,3} \\ \dot{\vec{x}}_{H,4} \end{bmatrix} = \begin{bmatrix} \vec{f}_L(\vec{x}_L, \vec{x}_{H,1}, \vec{x}_{H,2}, \vec{x}_{H,3}, \vec{x}_{H,4}) \\ \vec{f}_{H_1}(\vec{x}_L, \vec{x}_{H,1}) \\ \vec{f}_{H_2}(\vec{x}_L, \vec{x}_{H,2}) \\ \vec{f}_{H_3}(\vec{x}_L, \vec{x}_{H,3}) \\ \vec{f}_{H_4}(\vec{x}_L, \vec{x}_{H,4}) \end{bmatrix} \quad (5)$$

The system's state vector, $\vec{x}_S = \{ \vec{x}_L, \vec{x}_{H,1}, \vec{x}_{H,2}, \vec{x}_{H,3}, \vec{x}_{H,4} \}$, which is comprised of the load's 12 element state vector and four helicopter 21 element state vectors, is a 96 element vector. 60 state variables represent the slower dynamics of the helicopters and the load rigid body modes, coupled with the cables elastic tension. The other 36 state variables represent the main rotors faster dynamics. These two different time scales and the fact that the main rotors models are inherently stable, allows the dynamics and stability analysis to be performed using a reduced order model of the system. It can be observed that the four helicopters are coupled together through the load's state equations, as each helicopter's state functions are independent of the other helicopters state vectors. This feature of the system is a result of using the pendant configuration rather than using spreader bars. This creates an added difficulty in maintaining safe separation distances between the formation helicopters. As no structural coupling is physically present in the equations, it would have to be artificially added to the system through the controller algorithms.

A solution of the EOM starts from equilibrium. A trim state vector in the hover condition is found by setting all state derivatives to zero, and solving for the non-specified states and controls. Eqs (5) are then solved

through integration in time.

Note that a partial set of the equations introduced can be used for simulating the isolated load, or a single helicopter. For simulating the isolated slung load dynamics, the subsystem described by the first line in Eqs. (5) is used while setting cargo hook positions that are fixed in time. For simulation of a single helicopter without a load, any one of the other subsystems of Eqs. (5) can be used with zero cable forces. This technique allows the study of the influence of each dynamic component of the complex system on the resulting system's dynamic attributes.

2.5. System Simulation Model

A simulation model of the four rotorcraft multi-lift system was previously developed in MATLAB/SIMULINK [11]. This model was further enhanced by the inclusion of a detailed aerodynamic database of the load, the use of more realistic sling cable properties, and the capability of using a different model for each of the formation's rotorcraft. This last feature will enable the future simulation of mixed rotorcraft formations involving different helicopter models, or configuration variations of the same model.

Figure 5 shows the SIMULINK block diagram of the system's simulation model. The block diagram includes the four helicopter blocks, the load block, and the trajectory command generator block. The system's components physical connections are represented by the cable forces acting on the helicopters and the load. Each of the helicopter blocks includes subsystems describing the helicopter dynamics and controllers. The load block includes the load dynamics, and the cables force models. The trajectory control command generator block translates the required trajectory of the system into individual trajectory commands for each of the formation rotorcraft. These commands are used as inputs for the internal controller subsystems residing in each helicopter blocks.

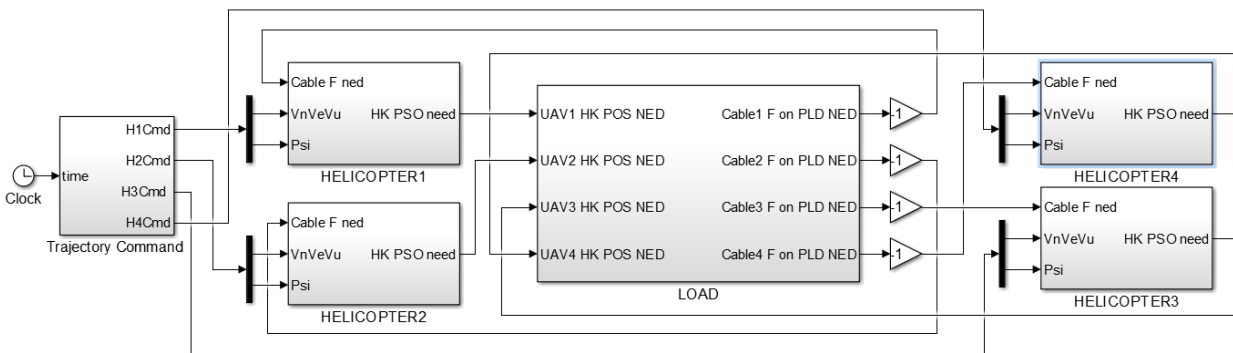


Fig. 5. SIMULINK model of the four helicopter multi-lift system

3. THE UNCONTROLLED SYSTEM DYNAMICS AND STABILITY DURING HOVER

The uncontrolled system's dynamics and stability characteristics during hover are studied using classic linear analysis methods. The analysis is performed for hover in order to facilitate the identification of the dynamic modes. First, the system's components (an isolated load "fixed to a ceiling", a single helicopter without an external load) are analyzed separately. Then, the complete system is analyzed. This allows the understanding of the coupling between the helicopters and the load and the identification of the unstable modes in the system and their nature.

3.1. Isolated Load Dynamics

Table 1 presents the six dynamic modes of the isolated load. Each mode corresponds to a pair of complex conjugate eigenvalues, representing very lightly damped oscillatory modes. Since the modal analysis is performed for zero airspeed conditions (conforming to hover), the load's aerodynamic forces and moments are negligible, and the single source for the damping present in the system is introduced by the cables. The corresponding mode shapes for the load are plotted in Fig. 6. The modal analysis shows that the mode shapes can be separated into two distinct groups: a "spring pendulum" modes group and a "rigid pendulum" modes group.

The first mode group expresses the structural coupling between the load's rigid body degrees of

freedom (DOF's) and the cables elastic properties. The three pairs of conjugate eigenvalues are characterized by a high natural frequency of 9.7-12.9 rad/s, and low positive damping of 2%-2.8%. These damping values reflect the cable damping ratio of 2.7% that was used for the cables models. The elastic mode shapes include a longitudinal pendulum mode, lateral pendulum mode, and a plunge mode. The longitudinal mode involves a forward/aft motion of the load's center of gravity coupled with pitch angle oscillations. Similarly, the lateral mode involves a right/left motion of the center of gravity coupled with roll angle oscillations. Interestingly, while for the longitudinal mode the pitch motion is in phase with the translational motion, for the lateral mode the angular motion is in opposite phase to the translational motion. Thus, a forward motion of the load is accompanied by a positive pitch up and a right motion is followed by a negative roll (right face up) motion. For an observer these two modes will appear the same, with the "leading" face climbing up. The load's plunge mode is a pure vertical motion mode. Its frequency of 11.1 rad/s is close to the approximate value of 11.55 rad/s calculated for a simple mass/spring harmonic system. In this simplified calculation, spring stiffness is equal to four times the cables stiffness in the vertical direction, and a mass equal to the load mass is used.

The second mode group reflects the mode shapes resulting from the load's inertia. The effect of the cables elasticity in these "rigid pendulum" modes is

Mode no.	Description	Eigenvalue [rad/s]	ω_n [rad/s]	ζ
1	1 st longitudinal ("elastic") pendulum	$-0.36 \pm 12.88i$	12.88	0.028
2	1 st lateral ("elastic") pendulum	$-0.19 \pm 9.69i$	9.69	0.02
3	Plunge mode	$-0.28 \pm 11.09i$	11.10	0.025
4	Yaw mode	$-4 \cdot 10^{-3} \pm 2.42i$	2.42	$1.6 \cdot 10^{-3}$
5	2 nd lateral ("rigid") pendulum	$-2 \cdot 10^{-4} \pm 1.06i$	1.06	$1.9 \cdot 10^{-4}$
6	2 nd longitudinal ("rigid") pendulum	$\sim 0 \pm 0.76i$	0.76	~ 0

Table 1. Isolated load dynamic modes, zero airspeed

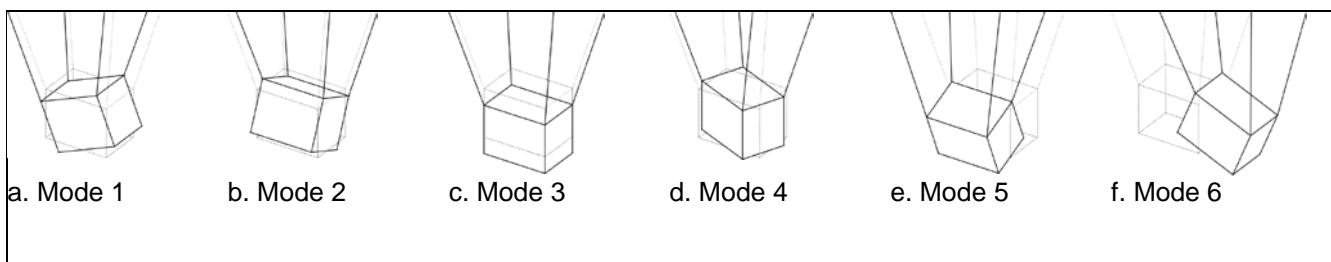


Fig. 6. Isolated load mode shapes, zero airspeed

very small so that these modes are practically very close to the ones that would result when using infinitely stiff sling cables. The three pairs of conjugate eigenvalues for this second mode group are characterized by a low natural frequency of 0.8-2.4 rad/s, and very low to negligible positive damping. The “stiff pendulum” mode shapes include longitudinal and lateral pendulum modes similar in shape to the respective elastic pendulum modes of the first group, and a pure load yaw mode. Compared to their elastic counterparts, the stiff longitudinal and lateral modes involve much larger translational components, and the angular motion of the load that is present in these modes is secondary. As cable tension is not significantly affecting these two modes, their damping ratio is practically zero. The phasing between the translational and angular components of the stiff pendulum modes is opposite from that described for the elastic modes: a negative pitch motion accompanies the forward translation for the longitudinal mode, and a positive roll motion (right face down) accompanies the rightward translation for the lateral mode. The pure yaw mode of the stiff pendulum mode group is created by the torsional stiffness effect of the cables tension forces. This mode is a result of the system’s geometry and not of the cables elasticity. However, due to the coupling between the load’s yaw and the cables stretch, the damping properties of the cables increase the modal damping of this mode.

The modal analysis results for the isolated load suggest that the main interaction between the helicopters and the load are expected to be reflected as low frequency oscillations of the “rigid pendulum” modes. This is owing to these modes being much closer in frequency to the helicopters rigid body modes, and their negligible damping in comparison the load’s elastic modes.

3.2. Helicopter Dynamics

Table 2 presents the modal analysis results for a single helicopter (not carrying a load). The high frequency pure main rotor modes (that are inherently stable and are practically uncoupled to the fuselage motion) are not presented since they are less significant for flight dynamics analysis. In addition, the four zero eigenvalue rigid body modes (expressing the uncoupling of the position and yaw angle degrees of freedom to the other equations of motion) are omitted as well.

The results show that the modes picture is similar to that generally expected for a hovering helicopter. The first three modes in the table (that are usually not studied in flight dynamics research) involve main rotor dynamics coupling with the fuselage degrees of freedom. These modes were included in table 2 for completeness. The other six modes are the “classic” longitudinal and lateral/directional modes described in helicopter flight dynamics literature. However, a significant change from these “classic” modes was noticed in the helicopter’s roll subsidence and airspeed modes (mode numbers 3,4). The helicopter’s longitudinal and lateral/directional dynamics are frequently analyzed separately, assuming these planes of motion are approximately uncoupled. The current analysis does not use this assumption. Analysis showed that the coupling between pitch and roll axis alters the classic roll subsidence mode such that it becomes a combined pitch/roll mode, with the pitch and roll angles having similar components in the mode’s composition. This coupling, that should be expected to exist for any conventional single main rotor helicopter is further intensified by the 20 deg canting of the Black Hawk’s tail rotor shaft. A change of tail rotor thrust due to a roll rate, will therefore be translated into both a pitching moment and a rolling moment, leading to a

Mode no.	Description	Eigenvalue [rad/s]	ω_n [rad/s]	ζ
1	Conning/Heave	-9.15	--	1
2	Lateral flapping/Roll	$-3.74 \pm 4.26i$	5.67	0.66
3	Roll subsidence	-5.89	--	1
4	Airspeed (Pitch) subsidence	-1.41	--	1
5	Hover pitch phugoid (“Falling leaf”)	$0.24 \pm 0.52i$	0.57	-0.42
6	Hover Lateral/directional phugoid (“Dutch roll”)	$-0.11 \pm 0.58i$	0.59	0.18
7	Yaw mode (Helicopter “spiral”)	-0.15	--	1
8	Heave	-0.27	--	1

Table 2. Single helicopter dynamic modes, hover

coupled change in both of these attitude angles. A change of tail rotor thrust due to a pitch rate will have a similar effect.

The single helicopter's modal analysis also shows that the only unstable mode is the pitch phugoid mode (also known as the "falling leaf" mode), corresponding to the divergent conjugate pair of pitch oscillation eigenvalues.

By comparing the eigenvalues of tables 1 and 2 it can be seen that the load's longitudinal and lateral frequencies are close to the helicopter's pitch and lateral/directional oscillations frequencies, so that the potential exists for a reduction in the stability of the system when all of its components are connected together.

3.3. System Dynamics

The system's modal analysis was performed using a reduced order model incorporating the 60 rigid body state variables of the helicopters and the load. The resulting model does not account for the faster dynamics of the main rotors (with 36 additional state variables), that have a low influence on the system's stability. Although geometrically the system appears symmetric, its dynamical characteristics are highly asymmetric and very complex. This is a direct outcome of the inherent coupling between the longitudinal, lateral and directional planes of motions for each helicopter. The trim attitudes of the formation helicopters are asymmetric (due to the need to counteract the tail rotor thrust forces). Thus, while the load and its four cables are trimmed assuming the symmetric geometric arrangement of Fig. 3, the resulting trim state vector for the helicopters does not show any specific pattern of either symmetry or anti-symmetry.

Table 3 presents the modal analysis results for the complete multi-lift system. The resulting system's modes can roughly be divided into three groups: modes originating from the isolated load dynamics (table 1), modes originating from the single helicopter dynamics (table 2), and modes that are created only when the helicopters and the loads are combined together. It should be stressed that in all of the modes, a coupling between the formation helicopters and the load is present to some degree. However, some modes can be more easily identified with the isolated load dynamics than others that are either helicopter dynamical modes influenced by the load, or helicopter/load new modes that have no trace in tables 1 and 2. A brief description of each mode group is given in what follows.

3.3.1. Modes Originating from an Isolated Load

All of the isolated load modes (listed in table 1) reappear as coupled load/helicopters modes in the system dynamics. Modes 1-3 and 9-11 correspond to

the "elastic pendulum" modes and "rigid pendulum" modes of table 1, respectively. The eigenvalues of the elastic modes are significantly distorted due to the use of a reduced order state-space model. The accurate results for these modes using an unreduced model result in frequencies of 12.8-14.3 rad/s (and damping ratios of 2.95%-3.64%) that are closer to these of the isolated load.

Both the elastic and rigid load modes show a substantial increase in damping characteristics following the attachment of the load to the rotorcraft. However, this is much more pronounced in the "rigid" pendulum modes, where sling cable damping effects are negligible. This observation regarding the increase in load damping following attachment to the rotorcraft is in agreement with previous experience with slung load carriage by a single helicopter. Flight tests have shown increased load damping during slung load carriage, as compared to damping values measured during dynamic wind tunnel tests [22]. This is explained by the added aerodynamic damping contributed by the helicopters main rotors that dissipate some of the load's kinetic energy. The helicopters are coupled to the load's motion so that load pitch and roll are accompanied by a similar motion performed by the formation's box corners. Thus the longitudinal pendulum modes are accompanied by the "pitching" of the formation box, where the leading and trailing helicopters are heaving in opposite directions. Similarly, the lateral pendulum modes involve a "rolling" of the box corners with the starboard and portside helicopters heaving in opposite directions.

All six modes of this group are stable for hover, where no contribution of the load's aerodynamic forces and moments to the system's dynamics is assumed. For forward flight, the modal analysis results are expected to change significantly. However, it is expected that the load related modes would remain stable due to two effects:

- The dissipation of the load's oscillatory kinetic energy by the helicopters.
- The limiting of the load's yaw oscillations by the sling cables stiffness, that eliminates the excessive yaw/roll load oscillations experienced during single carriage of similar box like bluff bodies.

These expectations have been later confirmed using nonlinear simulations of the system for a wide range of flight speeds.

3.3.2. Mode Originating from a Single Helicopter

These modes are similar in their dynamic nature to the single helicopter mode shapes. However, all of them contain significant components of load

Mode no.	Description	Eigenvalue [rad/s]	ω_n [rad/s]	ζ	
1	1 st Longitudinal ("elastic") pendulum + anti-symmetric helicopters heave (leading up/trailing down)	-0.031±33.405i	33.405	0.001	
2	Load plunge + helicopters conning/heave	-0.038±30.276i	30.276	0.001	
3	1 st Lateral ("elastic") pendulum + anti-symmetric helicopters heave (starboard up/port down)	-0.048±26.534i	26.534	0.002	
4	Load yaw + helicopters "diagonal" heave (2,4 up/1,3 down)	-0.142±15.537i	15.537	0.009	
5-8	Roll subsidence modes	-5.309	5.309	1	
9	2 nd Lateral ("rigid") pendulum + anti-symmetric helicopters heave (port up/starboard down)	-0.073±2.123i	2.124	0.034	
10	Load yaw + helicopters "diagonal" heave (1,3 up/2,4 down)	-0.006±1.994i	1.994	0.003	
11	2 nd Longitudinal ("rigid") pendulum + anti-symmetric helicopters heave (trailing up/leading down)	-0.085±1.483i	1.486	0.057	
12-15	Airspeed (pitch subsidence) modes	-1.313	1.313	1	
16-19	Hover pitch phugoid ("Falling leaf") modes	0.238±0.742i	0.779	-0.305	
20-23	Roll phugoid modes	-0.151±0.656i	0.673	0.225	
24	1 st Load spiral ("straight")	-0.007±0.372i	0.372	0.018	
25	2 nd Load spiral("diagonal")	-0.008±0.350i	0.350	0.023	
26-29	Yaw ("spiral") modes	-0.233	-0.148	0.148	1
		-0.215±0.025i			
		-0.121			
		-0.051±0.079i			
30-34	Yaw divergence/subsidence	0.090	0.042	0.042	-1
		0.061±0.056i			
		-0.052			
		0.045			
		0.047			
35	1 st Rigid body mode – formation yaw	-0.006	~0.	~0.	
36	2 nd Rigid body mode – formation "cross diagonal"	0.	0.	0.	
37	3 rd Rigid body mode – formation "rectangle"	0.	0.	0.	
38-40	4 th -6 th Rigid body modes – translation (3 principal directions)	0.	0.	0.	

Table 3. System dynamic modes, hover

translational motion in the longitudinal and lateral directions. This implies that the single helicopter related modes are coupled to load pendulum motions.

Unlike what was initially expected, the resulting helicopter modes are not merely the modes of table 2 repeating four times. The coupling between the system's components and the asymmetric loading conditions of the formation's rotorcraft lead to

complex mode shapes with changing and unequal weights of each of the formation's rotorcraft in each mode. Therefore, it was impossible to sort these modes on the basis of the most dominant rotorcraft, and they were combined in groups according to the most distinctive pattern of motion of each mode. In addition, these pattern of motions could not always be easily connected to their single helicopter "parents", as changes to both the mode composition, pole type

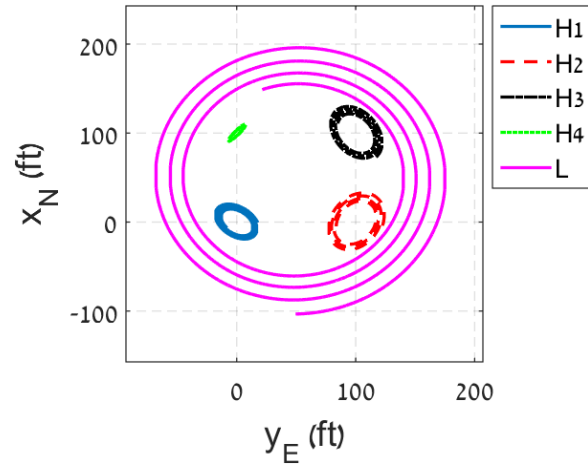
(real/imaginary) and number of similar group modes were occurring.

The results in table 3 show that similar to the single unloaded helicopter case, the main instability of the system around hover is governed by the four complex conjugate pairs of the pitch phugoid modes. The instability of these modes is reduced by the presence of the load, as can be observed by the modes average negative damping ratio of -3.05% as compared to -4.17% for the single helicopter case. The increase in damping is not a result of energy absorption by the load as in hover this dissipation is very small, and is originating in the cables elastic damping. It is probably caused by the dissipation of the unsteady motion of the dominant helicopter by the main rotors of the other helicopters of the formation.

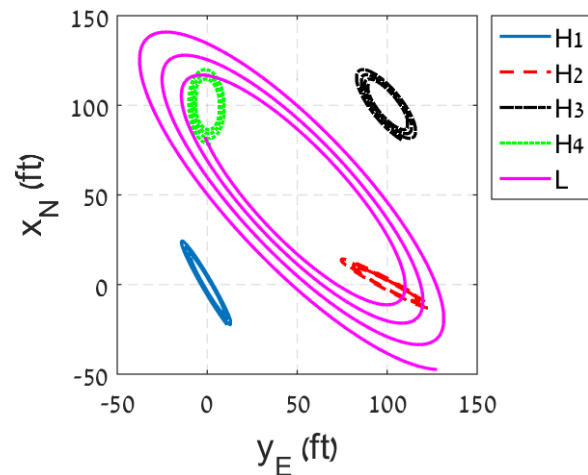
3.3.3. Helicopters/Load New Modes

The attachment of the system components created two mode types that could not be directly linked to the isolated components modes of tables 1 and 2. The first type of modes is an instability that is expressed as either a yaw divergence or a yaw phugoid, with times to double amplitude of 7.7s-15.4s. Although not as abrupt as the pitch phugoid instability, this yaw instability is still fast enough to adversely deteriorate the formation's rotorcraft flying qualities. Interestingly, unlike for the other modes group, the instability is more localized and is mostly expressed as a yaw divergence of the rear/left helicopter (no. 1) or a yaw phugoid of the rear/right helicopter (no. 2).

The second type of modes is expressed as a lightly damped load spiral motion. The two pairs of complex conjugate poles correspond to two principal directions of motion of the load, a longitudinal motion, and a diagonal motion. Figures 7a and 7b show the system's trajectory projected on the horizontal plane for the longitudinal and diagonal spirals, respectively. While these modes are stable, they can pose a significant problem both in terms of handling qualities and operational efficiency. The spiral shaped trajectory of each of the helicopters produces corresponding lateral and longitudinal accelerations of 0.1g and 0.15g, respectively, at the pilot seat. Despite the low frequency of the oscillation, these levels of acceleration would significantly degrade the rotorcraft handling qualities. The operational efficiency of the system can be expected to be influenced by the spiral trajectory of the load. Following deceleration to hover, the load placement procedure will have to be postponed until the load's spiral motions subside. With a time to half amplitude of 95 s, the operational consequences of these oscillations might be unacceptable. It should be noted that although the load's longitudinal and lateral rigid pendulum modes have similar damping ratios, they are not expected to cause similar problems as their time to half amplitudes is five times lower (less than 20 s).



a. Load longitudinal spiral mode



b. Load diagonal spiral mode

Fig. 7. Load spiral modes (hover)

3.4. System Dynamics and Stability – Summary

Figure 8 presents a root locus of the poles for the system's reduced order model. The isolated load's and single helicopter's poles are also plotted for reference. Red triangles represent system poles, black squares represent isolated load poles, and blue circles represent single helicopters poles. The rigid body modes were omitted from the plot for better clarity.

It could be seen that in general, the damping of the poles associated with the isolated load increase when the load is carried by the rotorcraft formation. All these modes turn more stable, although lightly damped. The modal analysis results have shown that despite their stability, these modes can create significant degradations in both hover handling qualities and operational efficiency.

The instabilities in the systems is twofold: the shorter period instability expressed as the pitch phugoid modes, and the longer period instability expressed as

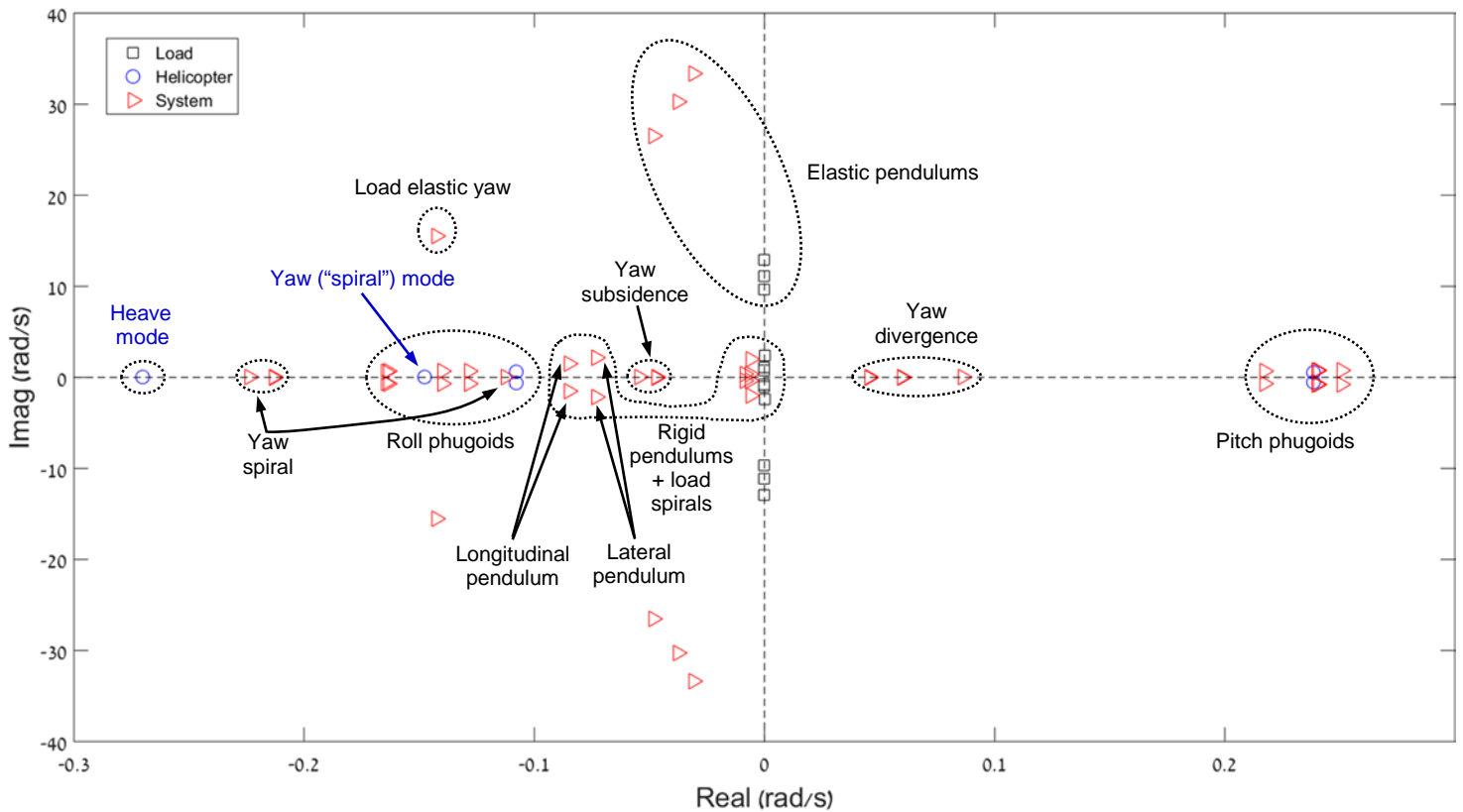


Fig. 8. Root locus of system poles (hover)

the yaw divergence/yaw phugoid modes. Since together these modes include components in all three planes of motion, it follows that a regulator must be included in the system in order to provide the required stability. Further, due to the complex interaction between all of the formation's rotorcraft, a controller would be required in order to provide a controlled and coordinated flight of all of the members of the formation. These tasks are being performed by a purposely designed control system that is described next.

4. FLIGHT CONTROL SYSTEM

4.1. Requirements and Structure

The multi-lift system's flight control laws should be able to fulfil the following requirements:

- Provide basic stability for each rotorcraft, with similar dynamic response characteristics.
- Provide moderate control commands to effectively follow the desired trajectory, while maintaining adequate control margins.
- Largely reduce the effect of the dynamic cable forces induced by load pendulum motions.
- Keep safe separation distances between the rotorcraft.

These requirements were met by the aerodynamic inverse controller introduced in Ref. [11]. However, this design required the direct measurement of cable forces to be used as feedback to the controller. Further, the implementation of the aerodynamic

inversion controller requires the use of detailed aerodynamic models of the helicopters components and of the load, and a real time inverse solution of the main and tail rotors models. Therefore, while providing the necessary performance, this controller design might prove too complex for implementation. It would also be inflexible in accommodating system configuration changes, specifically the change of the type of the carried load and its mass properties.

In order to simplify the controller's structure while meeting the stability and control requirements for the system, a new dynamic inversion (DI) controller was developed. The new controller implements a piecewise linear model of a single helicopter (without a slung load). This design eliminates the need for sling cables forces measurement for control feedback, and significantly reduces the inverted dynamic model's complexity. It provides the flexibility to use the same controller for both free flight without a load, and flight in multi-lift formations. The controller provides adequate robustness so that no specific knowledge of the carried slung load inertial and aerodynamic properties is needed. The top level DI controller block diagram for a single helicopter is shown in Fig. 9. This figure describes the dynamic model for the rear left helicopter (no. 1), but is essentially identical for all four rotorcraft. The required trajectory to be flown is used as the reference signal to the control system, and is initially identical for all the rotorcraft. The time dependent reference signal is composed of the the formation's desired inertial velocity vector given in the earth fixed (NED) coordinate system E , and the

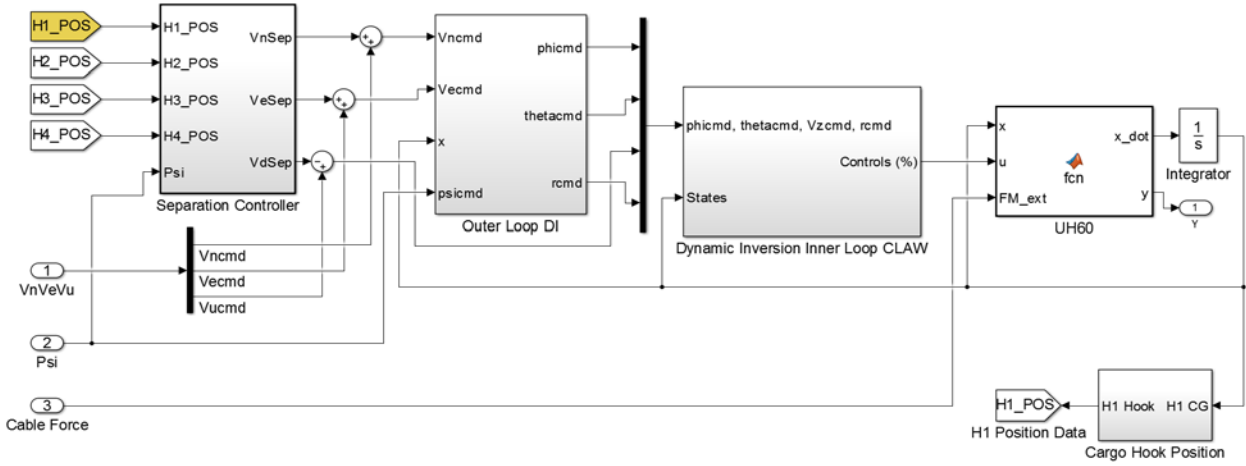


Fig. 9. SIMULINK control block diagram for helicopter no. 1.

formation's azimuth (yaw) angle.

The helicopter's DI controller is separated into three subsystems: an outer loop and inner loop dynamic inversion control laws, and a separation distance controller. These components would be elaborated next.

4.2. Dynamic inversion controller

The DI controller's role is the conversion of the trajectory required of the helicopter into a set of collective, cyclic and pedals control command. An external trajectory control command generator (to be described later) defines the required trajectory for each rotorcraft as a combination of a ground velocity vector and fuselage yaw angle. The outer loop DI controller processes this input and provides the inner loop DI controller with the required reference signal, \mathbf{r} :

$$\mathbf{r} = [\phi_{Hc}, \theta_{Hc}, \dot{h}_{Hc}, r_{Hc}]^T \quad (6)$$

where $\phi_{Hc}, \theta_{Hc}, \dot{h}_{Hc}, r_{Hc}$ are the required roll angle, pitch angle, rate of climb and yaw rate, respectively. The inner loop DI controller is implemented as a piecewise reduced order linear model of the helicopter:

$$\dot{\mathbf{x}} = \mathbf{A}\mathbf{x} + \mathbf{B}\mathbf{r} \quad (7a)$$

$$\mathbf{u} = \mathbf{C}\mathbf{x} \quad (7b)$$

where \mathbf{x}, \mathbf{u} are the reduced order state vector and the output control command vector, defined below:

$$\mathbf{x} = [u_H, v_H, w_H, p_H, q_H, r_H, \phi_H, \theta_H]^T \quad (8a)$$

$$\mathbf{u} = [\theta_{1c}, \theta_{1s}, \theta_0, \theta_{TR}]^T \quad (8b)$$

The coefficients matrices $\mathbf{A}, \mathbf{B}, \mathbf{C}$ are airspeed dependent, and were calculated using linearization of the single helicopter model about trimmed level flight conditions, spaced 20 Knots apart.

The inversion process is performed by defining a pseudo control vector, \mathbf{v} , so that:

$$\mathbf{u} = (\mathbf{C} \cdot \mathbf{B})^{-1} (\mathbf{v} - \mathbf{C} \cdot \mathbf{A}\mathbf{x} + \dot{\mathbf{r}}) \quad (9)$$

This results in a set of decoupled integrators for the tracking error dynamics, \mathbf{e} :

$$\dot{\mathbf{e}} = \dot{\mathbf{y}} - \dot{\mathbf{r}} = \mathbf{v} \quad (10)$$

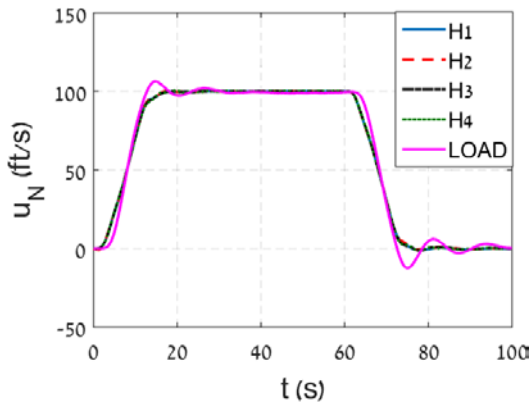
The linear system (10) of the error dynamics is controlled using a PID (proportional, integral and derivative) control law for \mathbf{v} , such that:

$$\mathbf{v} = -\mathbf{K}_P \cdot \mathbf{e} - \mathbf{K}_I \cdot \int \mathbf{e} dt - \mathbf{K}_D \cdot \dot{\mathbf{e}} \quad (11)$$

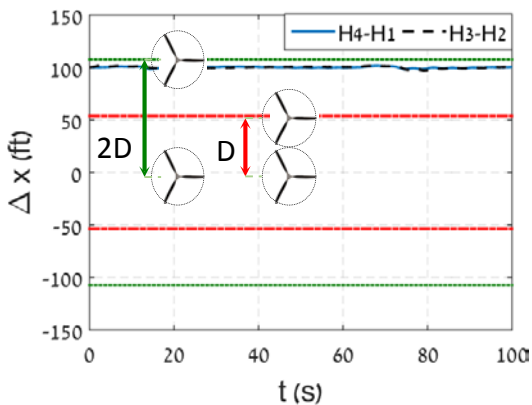
The gain matrices $\mathbf{K}_P, \mathbf{K}_I, \mathbf{K}_D$ are diagonal matrices, with their gains set to provide the required second order dynamic characteristics for the error dynamics.

It should be noted that while the linear model used in the DI controller is representative of a helicopter without a slung load, this model is still adequate for controlling the formation rotorcraft during slung load carriage. If a delicate flying technique is used and abrupt maneuvers are avoided, cables forces will be close to their trim value. Since the linearization results in a small perturbations model of the helicopter, the main effect of the cable forces can therefore be expected to show in the trim values, with the perturbations in cable loads treated as external disturbances to the system. In addition, the robustness of the DI method, and specifically the use of error integration in the control law for the pseudo control \mathbf{v} , compensates for the use of these approximate linear models of the helicopters.

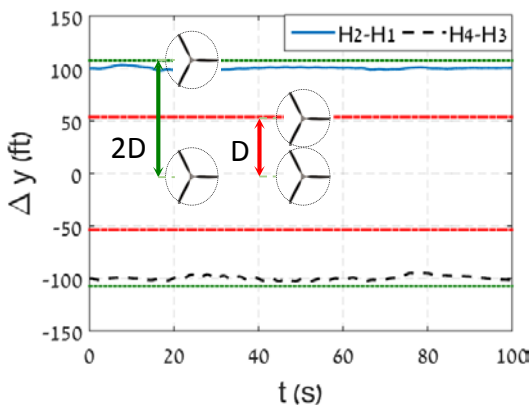
Preliminary simulation runs were first performed for acceleration-deceleration (accel./decel.) maneuvers along a straight line pointing north (along the \hat{x}_E axis). Figures 10 (a)-(c) present the inertial speed (u_N), and the longitudinal (ΔX) and lateral (ΔY)



a.



b.



c.

Fig. 10. Ground speed and separation distances for 100 ft/s accel./decel. maneuver

separation distances of the system for a 100 ft/s accel./decel. maneuver. These distances are defined as the longitudinal and lateral spacings between two adjacent helicopters: H3-H2 and H4-H1 for the right/left rotorcraft, and H4-H3 and H2-H1 for the lead/rear rotorcraft, respectively. Since the formation is flying due north, the lateral (v_E) and vertical (w_D) components of the formation's ground speed are very small. The red and green lines of figures (b) and (c) denote separation distances of one and two rotor disc diameters, respectively. A separation distance smaller than one diameter indicates an overlapping of

the tip path planes of two adjacent helicopters. As the helicopters are initially positioned at the corners of a 100x100 ft square, this distance (that is close to two rotor diameters) was chosen as the target separation distance for the current work.

The results show that the DI controller was successful in meeting the required goal, with all the helicopters following essentially the same flight path while maintaining their initial separation distance of 100 ft. Fig. 10 (a) shows the acceleration from hover (0s to 20s), 100 ft/s cruise (20s to 60s) and the deceleration back to hover (60s to 80s). Simulations were run for a range of airspeeds covering 40 ft/s to 200 ft/s in order to validate the controller's performance. Time history plots of the rotorcraft and load attitude angles

and of the rotorcraft control commands were checked in order to verify that attitude angles are not excessively high and that positive control margins exist.

4.3. Separation controller

The need for a dedicated control law for safe separation keeping was discovered during simulations that included either turns or low speed transitions with a sideward speed component. Results showed that in such maneuvers, or in any other maneuver where asymmetric disturbances were applied to the system, separation between the rotorcraft was no longer maintained by the DI controller. One such example is presented by Fig. 11 (a)-(c) for a "North-East" 14 ft/s transition maneuver. For this maneuver the formation is initially trimmed in hover so that it points north (zero yaw angle), and then transitions along a line directed north-east while maintaining its heading. Figure (a) shows the system's trajectory in the horizontal $\hat{x}_E - \hat{y}_E$ plane

(with \hat{x}_E pointing north and \hat{y}_E pointing south). It can be observed that although the formation generally flies in a north-east direction as required, the separation distances between the formation rotorcraft are not maintained. This is further demonstrated by Figs. 11 (b) and (c). Both the horizontal and lateral separation distances are reducing with time in the first part of the maneuver. The minimal horizontal separation distance reached is one rotor disc diameter (at 60s), the absolute minimum distance below which two rotor discs overlap. For the lateral separation distance, the minimum limit of one rotor disc is penetrated (57s to 61 s) with the two leading helicopters having a minimum separation distance of 0.62 rotor disc diameters, which is unacceptable. It is noted that the results presented in Fig. 11 were generated for a different slung load configuration than the nominal one (load weight of 30,000 lb, softer cables). Still, the results serve the purpose of demonstrating the need for a safe separation keeping

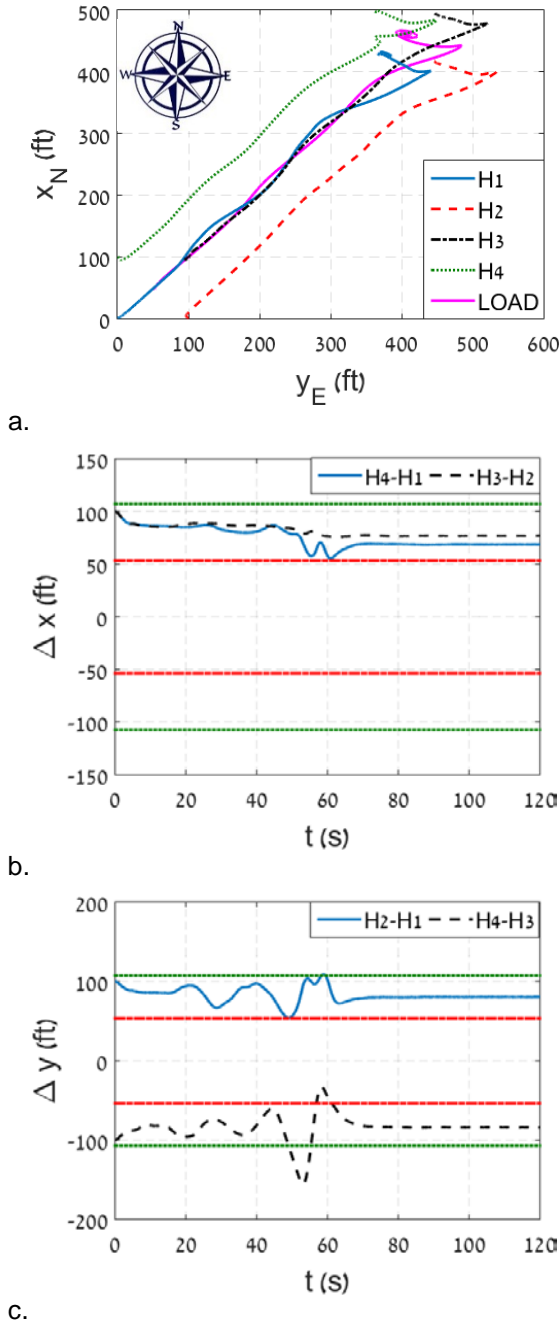


Fig. 11. Trajectory and separation distances during a "north-east" transition

function to be included in the controller. As noted above, similar results were also received when introducing disturbances into the system over a short period of time. Following these disturbances the rotorcraft would remain in their new disturbed separation distances, as no control mechanism was in place to drive them back to the desired separation distances.

The safe separation controller block was designed to provide corrective trajectory commands in response to changes in separation distances during flight (see

Fig. 9). For each helicopter the changes in separation distances with respect to each of the other formation helicopters are calculated. These changes are then averaged and fed into a PID regulator to provide an incremental velocity command. The incremental command is finally added to the formation trajectory command to provide the unique command for each helicopter of the formation.

The proper operation of the safe separation controller was validated by repeating simulations of maneuvers where separation distances limits were initially not maintained. The results showed that the separation controller was successful in providing adequate separation distances for the formation.

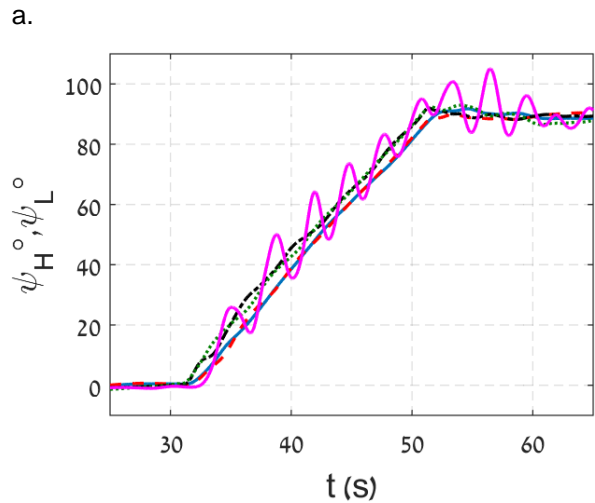
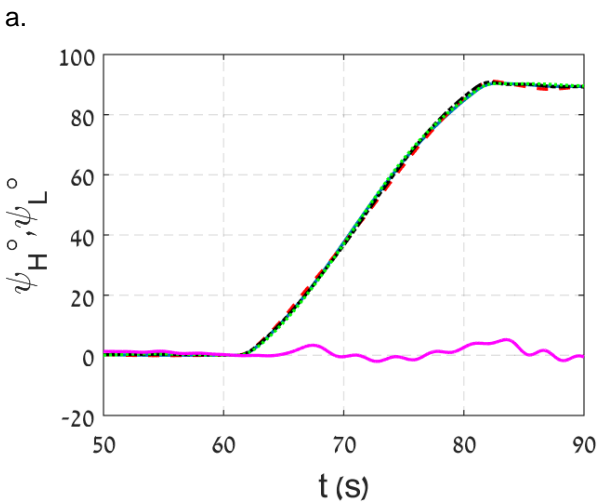
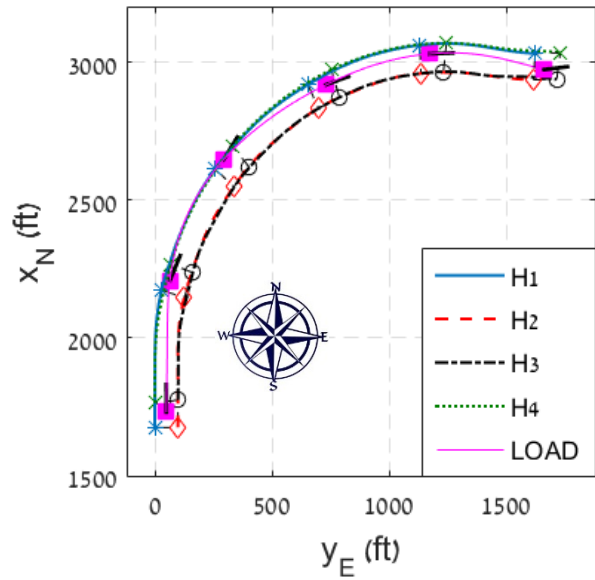
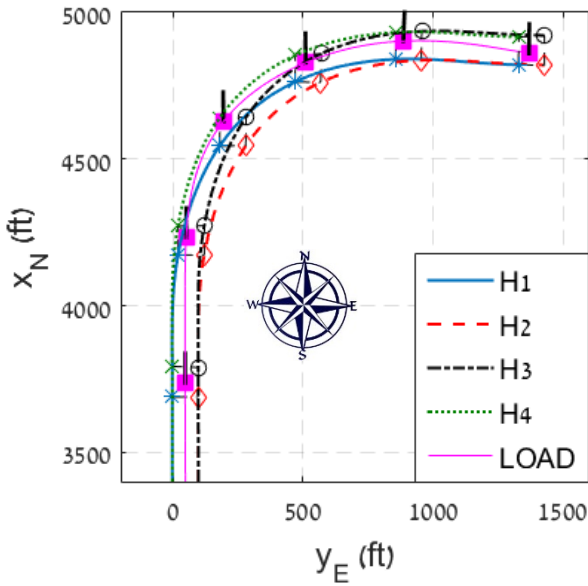
4.4. Payload/formation relative heading keeping

As explained earlier in section 2.1, it is assumed that the sling cables do not carry bending and torsion moments and that the cargo hook and load to cables attachment points are considered as spherical frictionless joints. In reality, unless the cargo hooks are swiveled, the cables are connected to the cargo hook and to the load attachment points through clevises. Therefore, relative yawing motions between the helicopters and the load result in cable torsion moments that are transmitted to the load through the cables attachment points. These moments play an important role during turns, as they drive the load to follow the formation's yaw angle.

Constant speed turns were simulated by using the following velocity vector as the commanded trajectory during the turn:

$$\begin{bmatrix} u_N \\ v_E \\ w_D \end{bmatrix} = V \begin{bmatrix} \cos(\dot{\chi}t) \\ \sin(\dot{\chi}t) \\ 0 \end{bmatrix} \quad (12)$$

Where V is the formation's velocity and $\dot{\chi}$ is the constant commanded turn rate. As the commanded velocity vector is identical for all four helicopters, the resulting trajectory flown by the formation is that of four parallel arcs with equal radii of curvature. This fact in combination with the lack of cable torsional moment led to the load keeping its initial yaw angle. This is demonstrated by Figs. 12a and 12b that show the formation's trajectory and the resulting yaw angles of the helicopters and load, respectively during a 100 ft/s right turn to the east. The markers in Fig. 12a indicate the helicopters and load position during five discrete times, and the black solid line shows the direction normal to the load's front face. As all the helicopters fly in parallel arcs, a rotation of roles of the helicopters occurs during the turn. Figure 12a shows that following the turn, H2 and H3 become the right/left lead helicopters, respectively, in place of H3 and H4. Likewise H1 and H4 become the right/left



b.
Fig. 12. Right turn maneuver, no turn compensation

b.
Fig. 13. Right turn maneuver, with turn compensation

rear helicopters, respectively, in place of H2 and H1. Figure 12b shows that while all the helicopters yaw 90 deg to the right as expected, the load keeps its front face pointing to the north so that instead of flying "narrow side on" it is now flying "broad side on". This change in formation arrangement is undesirable for two main reasons:

- 1) The respective roles of formation members during formation flight is usually determined based on operational considerations. For multi-lift missions (where cables forces are unevenly distributed among the helicopters) these roles might also be determined by considerations of the specific performance of each helicopter.
- 2) Flight with the load "broad side on" significantly increases the drag, thus increasing the power required for flight, and

reducing the attainable range and maximum flight speed.

In order to eliminate this problem, a turn compensation algorithm had been added to the trajectory command generator. This algorithm adds differential trajectory commands based on the rotorcraft positions, so that the resulting commanded trajectory will make the load yaw angle follow the formation's heading. The action of the turn compensation algorithm is demonstrated in Figs. 13a and 13b, for a similar turn maneuver as that shown in Fig. 12. Turn initiation times are different between these two figures, with initiation times of 61s and 31s for Figs. 12 and 13, respectively. It can be observed that with the turn compensation mode switched on, the load follows the formation's heading angle. The formation turns about an instantaneous centre of rotation, so that the leftward helicopters sweep a longer arc than the rightward ones (see Fig. 13a). The

lead helicopters yaw angles during the turn (Fig 13b) is about 4 deg to 6 deg larger than that of the rear helicopters. This difference in headings is what makes the load yaw to the right, as it is being pulled by the lead helicopters. The load's yaw oscillations apparent in Fig. 13b have a frequency of ~ 2 rad/s, which conforms to the load yaw mode described earlier in the modal analysis results (table 3, mode no. 10).

As the load yaw motion is restricted by cable stiffness, these oscillations are limited and are not of concern. The oscillations dampen out when the turn is complete and the helicopters return to straight flight.

5. RESULTS – SIMULATION OF A COMPLEX MANEUVER

5.1. Trajectory control command generation

The development process of the system's flight control laws was an on-going process, with modifications being introduced as deemed necessary by simulation results. Following the addition of each modification, the controller's performance was checked using simulations of both rectilinear and curvilinear maneuver sections such as: acceleration/deceleration, constant speed cruise, level turns, and climb/descent. Several such segments are now combined into a complex maneuver in order to verify the flight control system's capability to follow complicated and long maneuvers.

As explained earlier, the required maneuver sections to be flown were defined in terms of a three component inertial velocity vector in the NED inertial coordinate system E, and a formation yaw angle. While suitable for an engineering simulation, this form of trajectory specification is cumbersome for simulating a complex maneuver. As the system is intended to be evaluated in a real time simulator, the trajectory control command generation block was modified so that actual stick and pedal control commands are used for defining the formation's trajectory. While still allowing tabular input format to be used for non-realtime simulations, this modification allows the incorporation of the controller in a simulator for piloted real time simulations. The translation of stick, collective and pedals control commands to trajectory commands is airspeed dependent. A translational rate command (TRC) hover mode is implemented for airspeeds below 33.8 ft/s (20 knots) and an ACVH (acceleration command velocity hold) cruise mode is implemented for airspeeds above 67.5 ft/s (40 knots). Command blending is used for airspeeds in between, with gradual transition between the two modes. For both modes collective position is converted into a rate of climb/descent command, so that when the collective is in mid travel, zero vertical speed is commanded.

Pedals are used to command yaw rate for hover. In cruise mode, pedals command is translated into an offset heading command with respect the instantaneous velocity vector heading. A detailed description of the trajectory generator is beyond the scope of the current paper.

5.2. Maneuver description

The simulated complex maneuver is composed of basic mission segments. The maneuver starts from a trimmed hover out of ground effect (OGE), with the formation rotorcraft facing north. A level acceleration segment is then performed, followed by a constant speed level turn to the east. After the 90 deg right turn is completed a deceleration back to hover is performed. When back in hover, the formation yaws 90 deg to the right so that it is now facing south, and then transitions back. The maneuver ends with a hover OGE segment. The maneuver segments are

No.	Maneuver segment	Start time	End time
1	Trimmed hover OGE	0s	1s
2	Level acceleration	1s	22s
3	Level right turn to the east	22s	57s
4	Level Deceleration to hover	57s	80s
5	Right yaw to the south	80s	95s
6	Backward transition	95s	106s
7	Hover OGE	106s	120s

Table 4: Maneuver segments

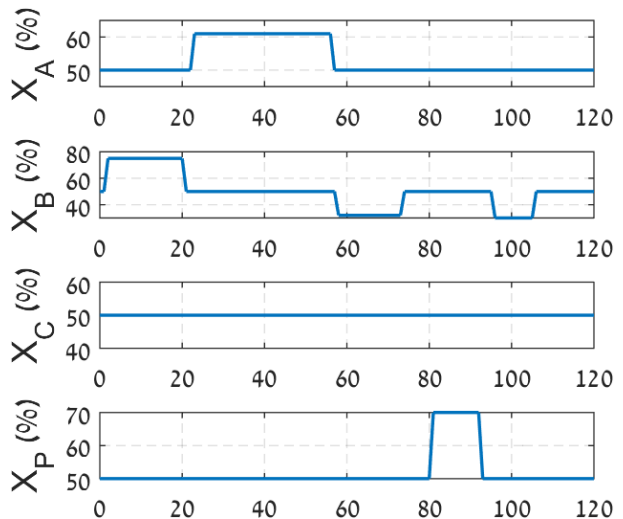


Fig. 14. Control commands

detailed in table 4 with the corresponding start and end times for each segment.

The control commands time history for the simulation is presented in Fig. 14. The longitudinal and lateral sticks, collective and pedals positions (noted X_A , X_B , X_C , X_P , respectively) are given in percent of the maximum control travel. As the demonstrated maneuver did not include any commanded altitude changes, the collective control position is held fixed at 50%.

5.3. Simulation results

Figures 15 a-f present time history results for the simulated complex maneuver. Figures 15 a and b show the 3D trajectory of the formation and its components, respectively. The data are presented using the earth fixed inertial coordinate system E. For better clarity, vertical position is presented in terms of altitude (negative direction of z axis of the system). The required trajectory is followed by all four rotorcraft, in response to the pilot's control commands of Fig. 14. Trajectory heading is shown to be swiftly changing between the segments, without noticing any accompanying hesitations, off axis drifts or oscillations of the ground track. Although no rate of climb is commanded through the collective, the altitude of the formation is seen to change. These changes are most apparent in the maneuver segments involving tilting of the main rotor disc: acceleration/deceleration and turns. The accelerated motion induces inertial forces in the load, that shift it from its equilibrium, and excite its pendulum modes. The coupling between the load pendulum motions to the rotorcraft heave create a pattern where the load's oscillations are accompanied by a slow descent of the formation, until the oscillations subside. The FCS control laws are designed to suppress the uncommanded vertical speed, but they do not include an altitude hold feature. Therefore, the drift in altitude is seen to be subsiding, but the rotorcraft do not automatically return to their initial altitude. It is noted that the current design of the FCS is intentionally minimal in order to allow manual flying of the system by a pilot. Therefore the development of more sophisticated and automated control laws is deferred to a later stage of the research.

The rotorcraft and load attitude angles are presented in Fig. 15c. The oscillation of the rotorcraft and load that were indicated earlier are clearly visible in the pitch and roll angles. Load yaw oscillations are also present, but are masked by the proximity of the rotorcraft yaw angle curves. The time history of the attitude angles shows that the FCS is successful in providing adequate stability for the formation, as the oscillations do not increase in magnitude during the turn, and die out once the turn is completed. Another important feature of the data is the uneven distribution of the load by the formation rotorcraft. This is outlined

by the differences in the rotorcraft pitch angles. During hover, the lead helicopters trim nose down, and the rear helicopters trim nose up. When the formation transitions into forward flight, the lead helicopters end up flying in a pitch angle that is 5 deg lower than that of the rear ones. This is a result of the geometric layout of the system, where the load's position between the lead and rear rotorcraft dictates that sling cable forces are pulling the lead helicopters back, and the rear helicopters forward. The resulting arrangement of the lead helicopters "dragging" the rear helicopters during forward flight is inefficient. Some of the power available to the rotorcraft is unnecessarily wasted in countering the sling cable forces, and as a result, the lead helicopter will reach their performance limits at airspeeds significantly lower than the rear ones. It seems that the geometric arrangement of formation rotorcraft should therefore be determined using performance optimization analysis, and possibly be airspeed dependent. We note that another problem that could be possibly alleviated using a better geometrical arrangement is that of the non-zero lateral load factors during flight. Sling cable forces aid in counteracting tail rotor thrust for the starboard helicopters while doing the opposite for the port helicopters. The balancing of these side forces is achieved through lateral tilting of the main rotor disc, which results in the flight being uncoordinated (non-zero lateral acceleration), both during the straight and level flight segments as well as in the turns.

Figure 15d presents the formation's ground speed components. The acceleration and deceleration segments show that velocity rate of change is monotonic and that the velocity profile is close to linear. Following the first acceleration segment, the formation reaches and maintains an average ground speed of 92 ft/sec (54.5 knots). As the system is flown using offline pilot control commands, the resulting trajectory is loosely defined. The deceleration segment back to hover is not completed prior to the initiation of the right yaw maneuver. Therefore the deceleration (indicated by the load speed) continues during the first part of the yaw. The rotorcraft longitudinal and lateral speed components during the right yaw segment (80s to 95s) demonstrate the operation of the yaw control law. The formation is turning about its geometrical center so that each of the rotorcraft follows a circular arc. The velocity vectors tangent to these arcs point in different directions, consistent with each rotorcraft relative position in the formation.

The longitudinal, lateral and total separation distances are presented in Fig. 15e. The separation controller is successful in maintaining the average separation distances very close to the 100 ft requirement (1.86 rotor diameters). The horizontal separation reaches a transient minimum of 84 ft (1.57 rotor diameters) during the hover transition to the

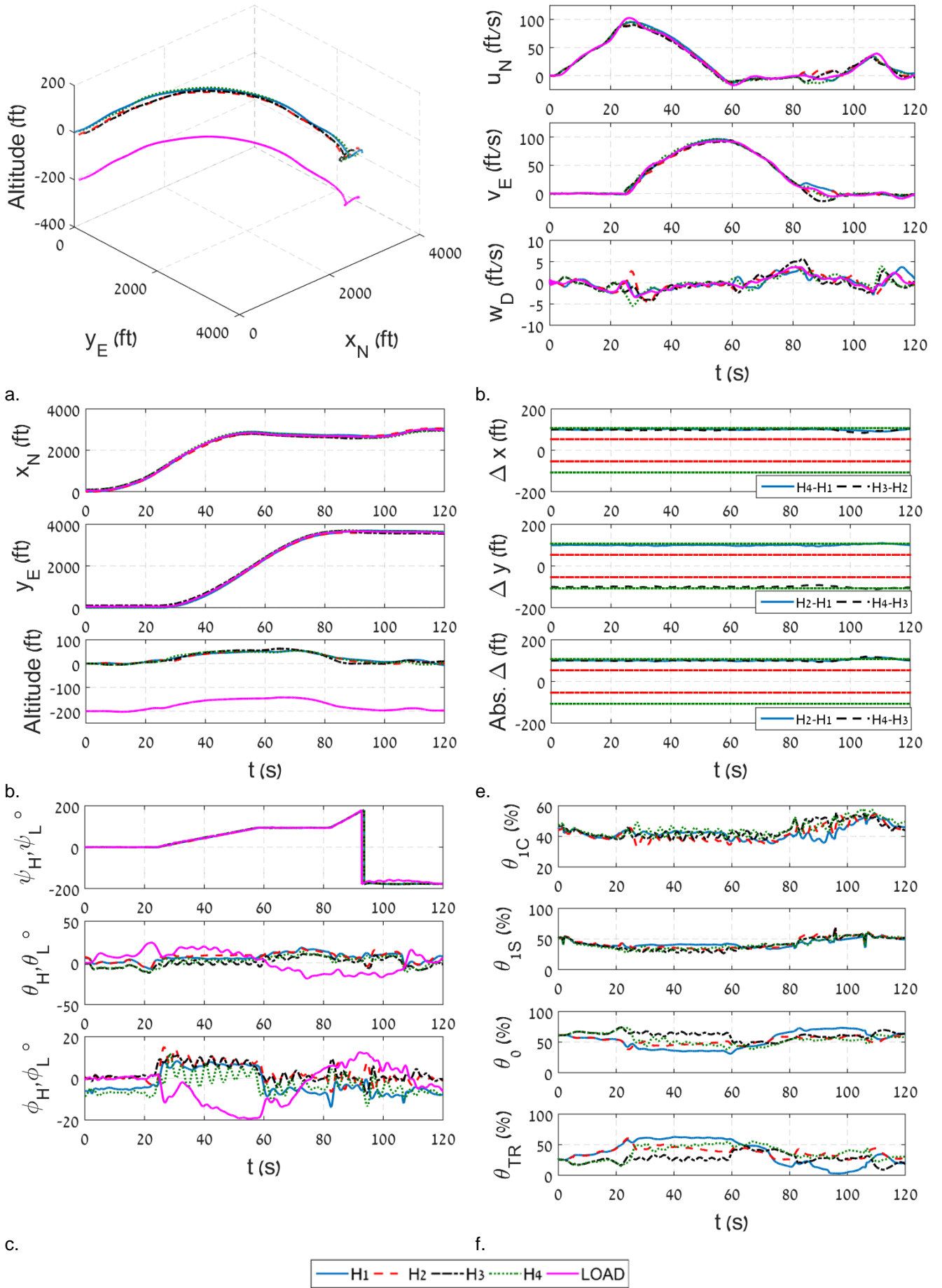


Fig. 15. Maneuver time history

back (104s). The lateral separation is at a transient minimum of 92 ft (1.71 rotor diameters) at 89s, during the right yaw segment. Nevertheless, the total separation distances between the helicopters are never lower than 94 ft throughout the entire maneuver. The closure rates (the relative velocities between the helicopters) are also low, with a maximum transient closure rate of 4.4 ft/s. Overall, the separation controller displays satisfactory performance, providing adequate separation between the formation rotorcraft, while keeping the separation dynamics slow and stable.

Finally, Fig 15f shows the control commands issued by the FCS to the formation rotorcraft. The data presented include the lateral cyclic (θ_{1C}), longitudinal cyclic (θ_{1S}), collective pitch (θ_0) and tail rotor pitch (θ_{TR}) for each of the helicopters. The collective pitch data reiterates the observation made earlier regarding the uneven load distribution. The higher collective pitch of the lead rotorcraft relative to the rear rotorcraft during the acceleration segment is clearly shown. When the formation enters the turn segment (22s into the maneuver) the two "branches" of the collective chart split further so that the collective pitch is increased for the two rotorcraft "inside" the turn and decreased for the opposite ones. This effect is a result of the increase in the airspeed of the portside helicopters, as they have to cover longer arcs during the turn. Since the formation's airspeed is below that for minimum power (the "bucket" speed), the airspeed increase of the portside helicopters leads to a reduction in the subsequent collective pitch angles. Similar indications to these described above can also be observed in the tail rotor pitch curves, which are an indication of the main rotors torques. These curves also show that the left pedal limit for the rear left helicopter is almost reached during the termination of the right yaw segment. It should be noted that these results were obtained using pedal limits that reflect the modified UH-60 tail rotor rigging used during high gross weight operation. The modified rigging increases tail rotor pitch by 3 deg so that tail rotor control travel is shifted by 10% to the left. This implies that performing the same maneuver with a helicopter that has not been re-rigged will result in the pedal limits being exceeded. This problem might be eliminated by avoiding the formation "box turning" pattern during hover, so that the rotorcraft will perform a pure yaw while holding their respective positions. Unlike the pedal commands, the longitudinal and lateral cyclic pitch commands are more limited in range, and use less than half of the available control travel. The time averages of these control commands are close to the stick centered position of 50%, so that stick control margins are high throughout the entire maneuver. Light oscillations of $\pm 4\%$ are observed in the lateral stick commands for the lead helicopters during the right turn segment. These oscillations are triggered by the action of the separation controller in response to the load's

pendulum modes that are excited during the entry into the turn. Although not of concern, the damping of these oscillations can be easily increased by a modified design of the separation controller.

6. CONCLUSIONS

The formation dynamics and control of a four rotorcraft multi-lift system was presented. The uncontrolled system was shown to be inherently unstable primarily due to the presence of coupled rotorcraft and load pitch phugoid modes. Load dynamic modelling was enhanced by the use of a detailed static aerodynamic database and more realistic sling cable properties.

A modified dynamic inversion controller for the coordinated flying of a multi-lift rotorcraft system was developed. The new controller does not require cable force measurement feedback, and provides a stable and controllable flight for the system, while keeping the rotorcraft safely separated.

The performance of the new controller was demonstrated for a formation of four UH-60 Black Hawk helicopters jointly carrying a 20,000 lb cargo container. The simulation of a complex maneuver including both hover and forward flight segments implied that the system can be successfully controlled by a single pilot. However, a better geometric arrangement of the system might be required in order to achieve a more efficient carriage and an even distribution of the load between the formation rotorcraft.

Follow-on planned activities include the performance of piloted real time simulations of the system, and an optimization of the system's geometry. These efforts will be conducted with the goal of improving system efficiency and handling qualities.

7. ACKNOWLEDGMENTS

This research was partially funded by the Government under Agreement No. W911W6-11-2-0011. The U.S Government is authorized to reproduce and distribute reprints notwithstanding any copyright notation thereon. The views and conclusions contained in this document are those of the authors and should not be interpreted as representing the official policies, either expressed or implied, of the U.S. Government.

8. REFERENCES

- [1] Curtiss, H. C. J. R., and Warburton, F. W., "Stability and control of the twin lift helicopter system," Journal of the American Helicopter Society Vol. 30, 1985, pp. 14-23.
- [2] Cicolani, L., and Kanning, G., "Equations of motion of slung-load systems, including multilift systems," NASA TP 3280, November, 1992.
- [3] Sheridan, P. F., "Feasibility Study for Multiple Helicopter Heavy Lift System," Vertol Aircraft Corp.,

- Philadelphia, PA, Report R-136, October 1957 (for U.S. Army Applied Technology Lab, Ft. Eustis, VA, Contract DA44-177-TC-391).
- [4] Meek, T., and Chesley, G. B., "Twin Helicopter Lift System Study and Feasibility Demonstration," Sikorsky Aircraft Co., Stratford, CT, Sikorsky Eng. Report SER 64323, December, 1970 (for U.S. Army Air Material Directorate, Ft. Eustis, VA, Contract DAAJ02-70-C0013).
- [5] Mittal, M., Prasad, J. V. R., and Schrage, D., "Comparison of stability and control characteristics of two twin-lift helicopter configurations," *Nonlinear Dynamics* Vol. 3, No. 3, 1992, pp. 199-223.
doi: 10.1007/bf00122302
- [6] Hess, R. A., and Tran, P. M., "Pilot/vehicle analysis of a twin-lift helicopter configuration in hover," *Journal of Guidance, Control, and Dynamics* Vol. 11, No. 5, 1988, pp. 465-472.
doi: 10.2514/3.20339
- [7] Raz, R., and Rosen, A., "Trim and stability of a twin-lift system in forward flight," *Journal of the American Helicopter Society* Vol. 50, No. 2, 2005, pp. 138-149.
- [8] Menon, P. K. A., Prasad, J. V. R., and Schrage, D. P., "Nonlinear control of a twin-lift helicopter configuration," *Journal of Guidance, Control, and Dynamics* Vol. 14, No. 6, 1991, pp. 1287-1293.
- [9] Mittal, M., and Prasad, J. V. R., "Three-dimensional modeling and control of a twin-lift helicopter system," *Journal of Guidance, Control, and Dynamics* Vol. 16, No. 1, 1993, pp. 86-95.
- [10] Cai, G., Chen, B. M., and Lee, T. H., *Unmanned Rotorcraft Systems*, Springer, 2011.
- [11] Song, Y., Horn, J. F., Li, Z., and Langealaan, J. W., "Modeling, simulation, and non-linear control of a rotorcraft multi-lift system," 69th American Helicopter Society International Annual Forum 2013, May 21, 2013 - May 23, 2013. Vol. 4, American Helicopter Society, Alexandria, VA, United States, 2013, pp. 2695-2714.
- [12] Horn, J. F., Guo, W. and Ozdemir, G. T., "Use of Rotor State Feedback to Improve Closed-Loop Handling Qualities," *Journal of the American Helicopter Society*, Vol. 57, No. 2, 2012, pp. 022001-1-10.
- [13] Krishnamurthi, J. and Horn, J. F., "Helicopter Slung Load Control Using Lagged Cable Angle Feedback," *Journal of the American Helicopter Society*, Vol. 60, No. 2, 2015, pp. 022011-1-12.
- [14] Spires, J. M. and Horn, J. F., "Multi-Input Multi-Output Model-Following Control Design Methods for Rotorcraft," American Helicopter Society International 71st Annual Forum, May 5 - 7, 2015, Virginia Beach, Virginia.
- [15] Li, Z., Horn, J. F., and Langelaan, J. W., "Coordinated Transport of a Slung Load by a Team of Autonomous Rotorcraft," AIAA Science and Technology Forum and Exhibition (SciTech). Washington, D.C., January 13-17, 2014.
- [16] Rosen, A., Cecutta, S., and Yaffe, R., "Wind Tunnel Tests of Cube and CONEX Models," Faculty of Aerospace Engineering, TECHNION - Israel Institute of Technology, TAE 844, November 1999.
- [17] Cicolani, L. S., Raz, R., Rosen, A., Gordon, R., Cone, A., Theron, J. N., Lusardi, J., Tischler, M., and Robinson, D., "Flight test, simulation and passive stabilization of a cargo container slung load in forward flight," American Helicopter Society International 63rd Annual Forum, May 1-3, 2007, Virginia Beach, VA.
- [18] Theron, J. N., Duque, E. P. N., and Cicolani, L., "A CFD Study of the Aerodynamics of a 6x6x8 Foot Cargo Container Suspended Beneath a Helicopter, Part I: Aerodynamics of the Stationary Container," US Army AFDD, AFDD/TR-07-001, October 2007.
- [19] Raz, R., Rosen, A., Carmeli, A., Lusardi, J., Cicolani, L., and Robinson, D., "Wind Tunnel and Flight Evaluation of Stability and Passive Stabilization of a Cargo Container Slung Load," American Helicopter Society International 64th Annual Forum, April 29 - May 1, 2008, Montréal, Canada.
- [20] Cicolani, L. S., Cone, A., Theron, J. N., Robinson, D., Lusardi, J., Tischler, M. B., Rosen, A., and Raz, R., "Flight test and simulation of a cargo container slung load in forward flight," *Journal of the American Helicopter Society* Vol. 54, 2009, pp. 0320061-03200618.
- [21] Cicolani, L. S., Lusardi, J., Greaves, L., LTC Robinson, D., Rosen, A., Raz, R., "Flight Test Results for The Motions and Aerodynamics of a Cargo Container and a Cylindrical Slung Load", NASA TP 2010-216380, Army TR-RDMR-AF-10-01, March 2010.
- [22] Raz, R., Rosen, A., Cicolani, L. S., Lusardi, J., Gassaway, B., and Thompson, T., "Using wind tunnel tests for slung loads clearance," 67th American Helicopter Society International Annual Forum, May 3-5, 2011, Virginia Beach, VA.
- [23] Raz, R., Rosen, A., Carmeli, A., Lusardi, J., Cicolani, L.S., Robinson, D., "Wind Tunnel and Flight Evaluation of Passive Stabilization of a Cargo Container Slung Load," *J. of the American Helicopter Society*, Vol. 55, No. 3, 2010, pp. 032001-1-18.
- [24] Howlett, J. J., "UH-60A Black Hawk Engineering Simulation Program: Volume I – Mathematical Model," SER 70452 (NASA Contractor Report 166309), December, 1981.
- [25] Gareth D. Padfield, "Helicopter Flight Dynamics: The Theory and Applications of Flying Qualities and Simulation Modelling," Washington DC: AIAA Inc., 1966.
- [26] Pitt, D.M. and Peters, D.A., "Theoretical Prediction of Dynamic Inflow Derivatives," *Vertica*, Vol. 5, No. 1, 1981, pp. 21-34.